Vertically-Oriented and Interpenetrating CuSe Nanosheet Films with Open Channels for Flexible All-Solid-State Supercapacitors

Lingzhi Li,[†] *Jiangfeng Gong,*[†,*] *Chunyan Liu,*[‡] *Yazhou Tian,*[†] *Min Han,*[‡,⊥,*] *Qianjin Wang,*[⊥] *Xihao Hong,*[⊥] *Qingping Ding,*[┘] *Weihua Zhu,*[†] *Jianchun Bao*[‡,*]

[†] Department of Physics, College of Science, Hohai University, Nanjing 210098, P. R. China

[‡] Jiangsu Key Laboratory of Biofunctional Materials, School of Chemistry and Materials Science, Nanjing Normal University, Nanjing 210023, P. R. China

[⊥] Nanjing National Laboratory of Solid State Microstructures, Nanjing University, Nanjing 210093, P. R. China

[┘] Ames Laboratory, US DOE, Ames, Iowa 50011, USA

Abstract: As a *p*-type multifunctional semiconductor, CuSe nanostructures show great promise in optoelectronic, sensing, and photocatalytic fields. Although great progress has been achieved, controllable synthesis of CuSe nanosheets (NSs) with desirable spacial orientation and open frameworks remains a challenge, and their use in supercapacitors (SCs) has not been explored. Herein, a highly vertically-oriented and interpenetrating CuSe NS film with open channels has been deposited on Au-coated PET substrate. Such CuSe NS film exhibits high specific capacitance (209 F g^{-1}) and can be employed as a carbon black- and binder-free electrode to construct flexible, symmetric all-solid-state SCs using polyvinyl alcohol (PVA)-LiCl gel as the solid electrolyte. A device fabricated with such CuSe NS films exhibits high volumetric specific capacitance (30.17 mF cm^{-3}), good cycling stability, excellent flexibility and desirable mechanical stability. The excellent performance of such device results from vertically-oriented and interpenetrating configuration of CuSe NS building blocks, which can increase available surface and facilitate the diffuse of electrolyte

ions. Moreover, as a prototype for application, three such solid devices in series can be used to light up a red LED.

Keywords: Nanosheets, orientation, interpenetration, electrodeposition, copper selenide, solid-state supercapacitors, flexibility

INTRODUCTION

Supercapacitors (SCs) have been playing an important role in high performance power sources due to their fast dynamic response, high power density, and excellent cycling stability in comparison with secondary batteries and dielectric capacitors.[1-4] Recently, with the ever-increasing demand for developing flexible energy storage devices for use in portable and wearable electronics, flexible all-solid-state SCs have attracted much attention.[5-8] For this purpose, the key lies in finding proper electro-active materials with good mechanical properties and intergrating them into special device configurations. During the past decades, two kinds of electro-active materials have been widely studied. One are carbon-based materials (*e.g.* carbon nanotubes,[9,10] activated carbon,[11,12] graphene,[13-15] *etc*.). The other are transition metal oxides/hydroxides (*e.g.* RuO_2,[16-18] V_2O_5,[19] MnO_2,[20-22] $Ni(OH)_2$,[23-25] $Co(OH)_2$,[26] *etc*.). These electro-active materials have their merits and drawbacks. The former ones are very stable, but their specific capacitances are relative low due to the limitation of electronic-double-layer energy storage mechanism. The latter ones possess high theoretical capacitance, whereas their electrical conductivity and mechanical properties are poor. The intrinsic shortcomings of these electro-active materials suppressed to develop high-performance flexible, all-solid-state SCs. To overcome those limitations, exploring novel

electro-active materials or materials combination is urgently needed and still remains a challenge in current materials science.

With the structure similar to graphene, two-dimensional (2D) layered metal chalcogenides (LMCs) nanostructures, such as few-layered VS_2 nanosheets (NSs),[27] metallic MoS_2 NSs or films,[28-30] WS_2 NSs,[31] Cu_2WS_4 NSs,[32] SnSe NSs and $SnSe_2$ nanodisks (NDs),[33] have been found to be novel electro-active materials for flexible SCs due to their high surface area, good electrical conductivity and excellent mechanical properties. As a member of LMCs family, CuSe has been identified as a *p*-type multifunctional semiconductor, and is widely used in solar cells,[34,35] gas sensors,[36] photodetectors,[37] and photocatalytic fields.[38] However, its strong interlayer chemical bonding makes it hard to obtain 2D CuSe NSs or NDs *via* conventional "top-down" strategy, *i.e.*, mechanical or liquid-assisted exfoliation of bulk crystals. On the contrary, the "bottom-up" route may be an ideal choice. By far, some "bottom-up" strategies, such as hydrothermal,[38] colloidal chemical route,[39,40] microwave-assisted wet chemical synthesis,[41] metal ions mediated morphology and phase transformation method,[42] have been developed to synthesize CuSe NSs or NDs. Despite great progress that has been achieved, fabricating 2D CuSe NSs or NDs with desirable spacial orientation and open channels remains a challenge, and their use in SCs field has not been explored.

In this paper, a novel 2D CuSe NS film has been successfully fabricated on Au-coated PET substrate through a facile electrodeposition method, and employed as electro-active materials for flexible, all-solid-state SCs. The detailed synthetic procedure is shown in the experimental section. Such CuSe NS film possesses the following significant features: (1) All CuSe NSs

are almost vertical to Au-coated PET substrate and interwoven to form free-standing film with macro-pores or large open channels. Such configurations not only can inhibit the re-stacking of CuSe NSs and fully utilize their surface but also offer many open channels for the diffusion of electrolyte ions to electrode surface; (2) The intrinsic good electrical conductivity[40] of the CuSe NS building blocks make such NS films can be directly used as carbon black- and binder-free electrode to fabricate flexible SCs; (3) Such CuSe NS film has a good contact with Au-coated PET substrate, which can efficiently reduce contact resistance and improve electron transfer efficiency. In a three-electrode system using 1M Na_2SO_4 aqueous solution as the electrolyte, the specific capacitance of such CuSe NS film can reach 209 F g^{-1} at a current density of 0.2 A g^{-1}, which is comparable to or higher with other reported materials (*e.g.*, graphene (G)-Mn_3O_4 nanorods,[43] N-doped ultrathin carbon NSs,[44] *etc*.). Due to its high specific capacitances, such CuSe NS film is further employed to construct flexible, all-solid-state SCs (CuSe NS-SSCs). The fabricated CuSe NS-SSCs device exhibits high volumetric specific capacitance (30.17 mF cm^{-3}), good cycling stability, excellent flexibility and desirable mechanical stability, indicating that the CuSe NS film is an enticing candidate material for use in high performance, flexible, all-solid-state SCs. Moreover, as a prototype for practical application, three such solid devices in series can be employed to light up a red LED.

RESULTS AND DISCUSSION

To obtain high-quality CuSe NS film, electrodeposition parameters (deposition potential, temperature, and time) are firstly optimized. The details are given in the supporting information **(**SI**)**. Though the CuSe NS films can be obtained at a wide range of deposition potentials, their qualities are quite different. For example, when the deposition potential deviates from -0.15 V (*vs.* SCE) (SI, Figure S1), the edge length of the CuSe NS building blocks is not uniform and their thickness becomes larger. In addition, as the deposition temperature is lower than 60 ºC, the crystallinity of the sample will be reduced accompanied with the generation of some Se nanoparticles on the surface of the sample (SI, Figure S2). Beyond deposition potential and temperature, the deposition time is found to greatly affect the loading amount and thickness of the obtained NS film (SI, Figure S3). The above experiments implied that the optimal conditions are deposition potential of -0.15 V (*vs*. SCE) at 60 ºC for 30 minutes.

The microstructures of the CuSe NS films obtained at the optimal deposition conditions are characterized by SEM and TEM. From the top-view low magnification SEM image (**Figure 1**a), a large-area uniform film can be clearly observed. The related high-magnification SEM image (Figure 1b-c) reveals that such film is composed of well-arranged NSs with edge lengths of about 1μm. Moreover, those NSs building blocks are almost perpendicular to the substrate and interwoven to form a free-standing film with large open channels. As measured from Figure 1c, the average thickness of those CuSe NS building blocks is about 15 nm. The related side-view SEM image (Figure 1d) analysis confirms that the whole film is vertical to the substrate, and its height is estimated to be about 4 μm. Further microstructure analysis of

such CuSe NSs is performed by TEM. The typical TEM image (Figure 1e) reveals that the primary building blocks of such NSs are irregular sheet-like nanostructures. The dark contrast results from the overlap or interpenetration of the NSs building blocks, confirming the interpenetrating structure of the NS film. The related HR-TEM image (Figure 1f**)** of an individual NS building block exhibits clear lattice fringes with the spacing of 3.46 and 3.46 Å, corresponding to the interplanar separation of (100) and (010) planes of klockmannite CuSe (JCPDS card: 34-0171), respectively. The intersection angle of these two planes is measured to be 120^{o}, which is identical to the theoretical value between the (100) and (010) planes. These results indicate that the top and bottom surfaces of the CuSe NSs building blocks are {001} surfaces. The corresponding selected area electron diffraction (SAED) pattern shows clear diffraction spots, revealing the NSs building blocks have single-crystalline structure. Further X-ray energy dispersive spectroscopy (EDS) was also performed to confirm the component of the NSs building blocks. The related EDS pattern is shown in Figure S4a. The peaks at 11.21, 12.50, 1.38 and 1.42 keV correspond to the K_{α}, K_{β}, L_{α}, L_{β} emissions of selenium, respectively. The other peaks located at 8.04, 8.907 and 0.92 keV are assigned to the K_{α}, K_{β}, L_{β} emissions of copper, respectively. By integration calculation, the atomic ratio of Cu and Se is close to 1:1, implying that the NS may be CuSe. To evaluate the loading amount of the CuSe NSs active materials, the cathodic charge *vs* deposition potential plots are provided in SI, Figure S4b. Based on Faraday's Second Law, the deposited mass of the CuSe NS film is calculated (SI e1) to be about 0.65 mg cm^{-2}.

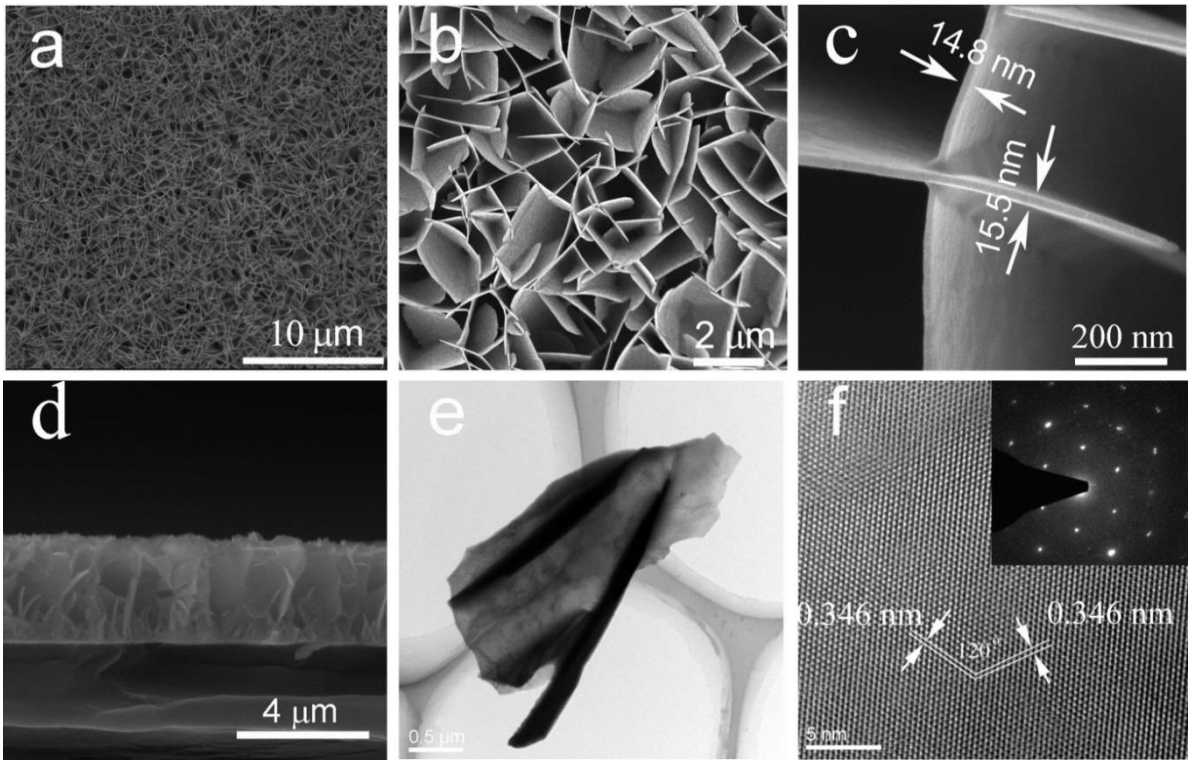

Figure 1. (a-c) Top-view low and high magnification SEM images of the CuSe NS film obtained at optimal deposition conditions. (d) Side-view SEM image of such CuSe NS film. (e) Representative TEM image of such CuSe NS film. (f) Corresponding HR-TEM image and SAED pattern of an individual NS building block in such CuSe NS film.

The constituents, phase structure and crystallinity of the obtained CuSe NS film are examined by X-ray diffraction (XRD), Raman spectroscopy and X-ray photoelectron spectroscopy (XPS). **Figure 2**a shows the corresponding XRD pattern. Excluding the diffraction peaks labeled with asterisks at 25.94° and 38.24° that originate from Au-coated PET substrate, two main diffraction peaks located at 28.06° and 46.05° can be observed, which are indexed to (102) and (110) planes of CuSe with hexagonal klockmannite phase structure (JCPDS No. 34-0171). No diffraction peaks of other impurities are found in the XRD pattern, indicating that the product is pure CuSe. Raman spectrum is also performed to

identify the constituents of the product as shown in figure 2b. The most intense peak centered at 256.7 cm^{-1} is attributed to the stretching mode of Cu-Se bond of klockmannite CuSe , the other peak located at 237.5 cm^{-1} corresponds to the Se-Se vibration model. [45] In addition, the broad shoulder at 135-203 cm^{-1} region may imply the existence of a metastable multi-phase in relation to polycrystalline Cu-Se compound at its surfaces.[45] Moreover, to identify the valence states of Cu and Se elements, XPS analysis is further carried out. From the XPS spectra of Cu 2p (Figure 2c), the binding energy (BE) of Cu $2p_{3/2}$ peak is observed at 932.4 eV, which can be attributed to Cu^{2+} ions. At the BE of 934.7 eV, a weak characteristic satellite peak for Cu^{2+} ions also can be seen, confirming that the valence state of Cu is +2. [46,47] Figure 2d shows the XPS spectrum of Se 3d, the peak at the BE of 55.1 eV is corresponding to the characteristic Se $3d_{5/2}$ of Se^{2-} ions, proving that the valence state of the Se element is -2. These results demonstrate that the deposited product is pure CuSe. [46,47]

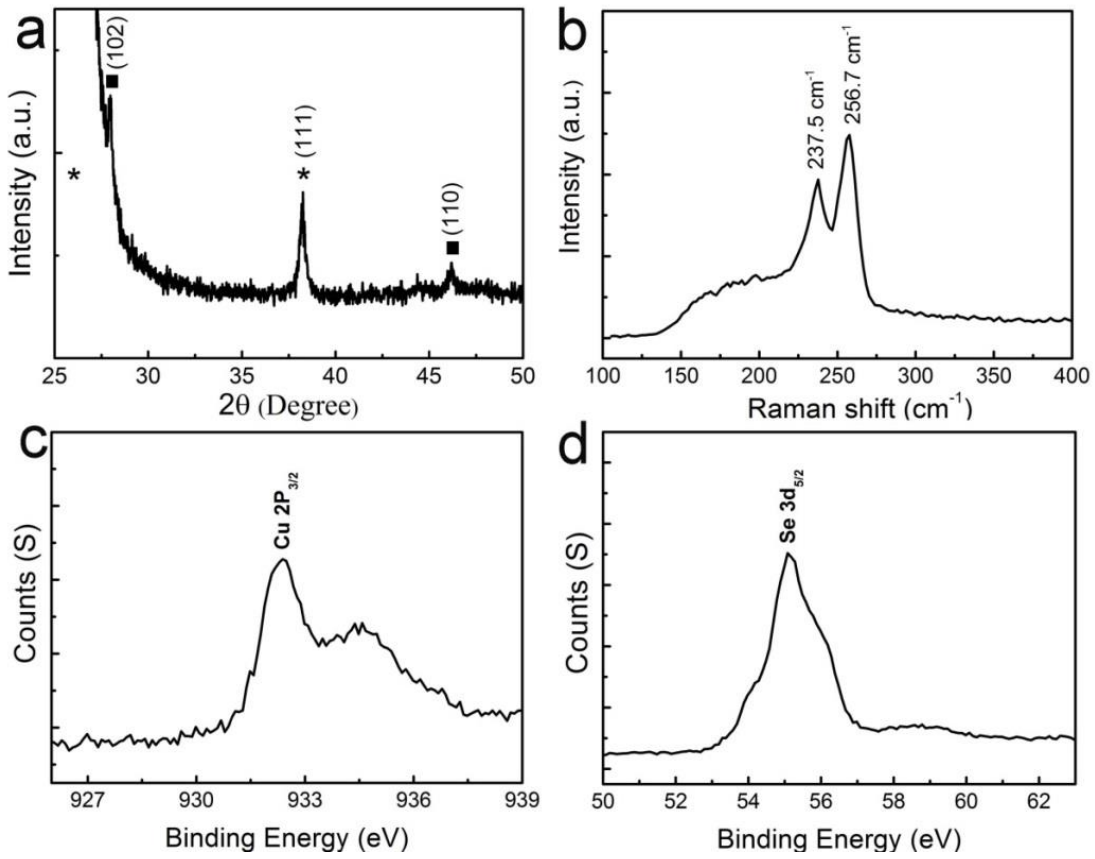

Figure 2. (a-b) XRD pattern and Raman spectrum of the CuSe NS film obtained under the optimal deposition conditions. (c-d) Corresponding XPS spectra for Cu 2p and Se 3d regions of the obtained NS film.

The electrochemical properties of the CuSe NS film obtained at optimal deposition conditions are firstly evaluated in a three-electrode system using 1M Na_2SO_4 aqueous solution as the electrolyte. **Figure 3**a shows the CV curves of the CuSe NS film at different scanning rates and Au-coated PET substrate at a scan rate of 100 mV s^{-1}, respectively. The much larger CV pattern observed on the former integrated electrode reveals that its capacitance is much higher than that of the latter, and the contribution of substrate to the total capacitance of the integrated CuSe NS film electrode can be neglected. It can be seen that the shapes of the CV

curves for such CuSe NS film are nearly unchanged as the scan rates increase from 10 to 200 mV s^{-1}, implying improved mass transportat, excellent electronic conductivity within the nanostructures, and small equivalent series resistance.[23] Galvanostatic charge-discharge (CD) measurements were performed to explore the potential applications of such CuSe NS film as electrode active-material (Figure 3b). From the discharge curves, the specific capacitances of the CuSe NS film at various current densities can be calculated (SI e2-e3). As illustrated in Figure 3c, the maximum specific capacitance of such CuSe NS film is 209 F g^{-1} at the current density of 0.2 A g^{-1}, which is higher than or comparable to those of recently reported MnO_2 nanocomposites,[22] $SnSe_2$ nanodisks,[33] graphene(G)-Mn_3O_4 nanorods,[43] N-doped ultrathin carbon NSs,[44] rGO-CoS_2 nanohybrids,[48] hierarchical $MnMoO_4$/$CoMoO_4$ heterostructured nanowires,[49] and cobalt phosphaste ultralong nanoribbons based microarchitectures.[50]

The long-term cycling stability of the CuSe NS film electrode is evaluated through Galvanostatic CD cycles at a current density of 1.0 A g^{-1}. As shown in figure 3d, the CuSe NS electrode exhibits stable electrochemical performance during the long-term testing, and the capacitance retention is 58.3% after 10000 cycles. The first five and the last five CD curves are shown in Figure S5a-b. The good cycling stability of the CuSe NS film may be related to its stable microstructure, using SEM to analyze the sample after cycling tests, we find that the CuSe NS film only exhibit slight variation in its microstructure (SI, Figure S5c).

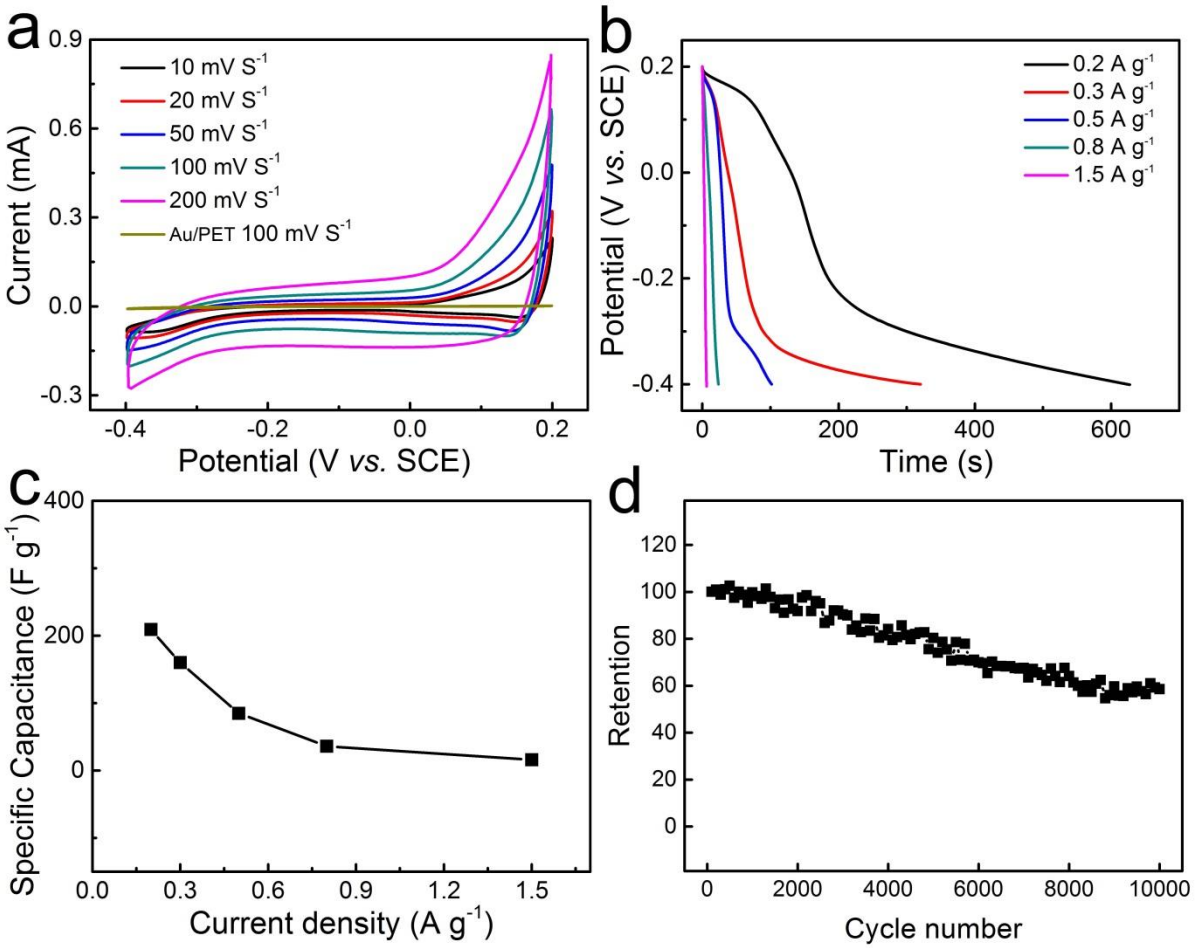

Figure 3. Electrochemical characterization of the CuSe NS film on Au-coated PET substrate for SCs in a three-electrode system. (a) CV curves of the CuSe NS film at different scanning rates and the Au/PET substrate scanned at 100 mV s^{-1}. (b) Galvanostatic discharge curves at different current density. (c) Specific capacitance *versus* current density plot. (d) Cycling performance of the CuSe NS film electrode.

For safety and portable consideration, all-solid-state SCs are superior to their counterparts with liquid electrolytes, which need robust encapsulation to prevent leakage of liquid electrolyte. Stacked symmetric all-solid-state SCs are further fabricated using the CuSe NS film obtained at optimal deposition condition as the active material, which are named and abbreviated as CuSe NS-SSCs. The polymer-gel (polyvinyl alcohol (PVA)-LiCl) served as

both the separator and the solid-state electrolyte. **Figure 4**a shows the detailed configuration of the solid device. For the actual solid device, the working area is 3 cm^{-2} and the thickness is 0.035 cm. The volume of the whole device is calculated to be ~0.105 cm^3. The CV profiles (Figure 4b) of the CuSe NS-SSCs device show obvious redox peaks at the scan rate ranging from 10 to 200 mV s^{-1}, indicating an ideal pseudo-capacitance behavior that is attributed to the surface adsorption of Li^+ ions and the fast reversible surface redox reactions. Moreover, galvanostatic CD tests of the solid device were performed and the discharging branch curves are shown in Figure 4c. The observed linear voltage-time profiles without obvious IR drop demonstrate a low internal resistance and an excellent capacitive performance of the solid device. Calculated from Figure 4c **(**SI e4**)**, the volumetric specific capacitances of the solid device are 30.17, 16.64, 13.83, 10.07, 7.41, 7.09 and 6.74 mF cm^{-3} at the volume current density of 0.14, 0.23, 0.29, 0.43, 0.57, 0.86 and 1.14 mA cm^{-3}, respectively (Figure 4d). The excellent energy storage performance of our solid device may be attributed to the vertically-oriented and interwoven configuration of the active CuSe NS materials that form macro-pores or open channels, facilitating the adsorption or diffusion of electrolyte ions for faradaic redox reaction. Even so, the specific capacitance of CuSe NS film based all-solid-state device is much lower than that tested in Na_2SO_4 aqueous solution, the phenomenon is very common in other active-materials, which is mainly attribute to the diffuse ability of the ion at two different electrolytes. In the solid device, the PVA- LiCl gel electrolyte dispersed on the surface of CuSe NS and became solid gradually due to the evaporation of the excess water, the diffuse ability of the ion in the solid medium is much

lower than that in aqueous solution, which would reduce the redox reaction level at the surface of CuSe NS, and finally changed its specific capacitance for granted. Additionally, the CuSe NSs active materials contact well with the current collector, which can reduce the contact resistance and offer another positive contribution to fast electron transport in the solid device. . The cycling stability of the CuSe NS-SSCs device is further evaluated by cyclic CD process at constant current density. After continuously operating for 10000 cycles, the CD curves of the solid device are still highly symmetry (SI, Figure S6), indicating good electrochemical stability and capacitance retention ability. Figure 4e shows the plot of the volume specific capacitance *versus* the cycling number. At the volume current density of 0.57 mA cm^{-3}, 90 % of initial capacitance value can be reserved after 10000 cycles, revealing the excellent cycling stability of the solid device. Moreover, to explore the possibility for practical application, three such solid devices are connected in series with the dream to drive a red light-emitting diode (LED) (1.8 V, 2 mA). As shown in Figure 4f, the red LED can be lighted for 3 minutes after being charged at 40 μA cm^{-2} for 150 s.

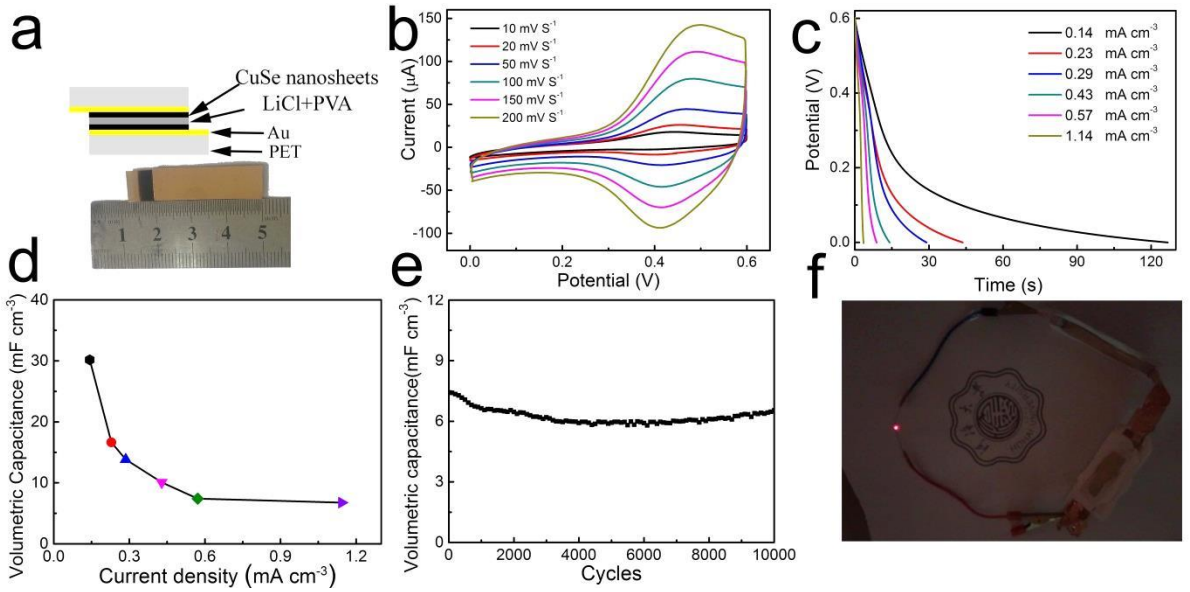

Figure 4. (a) Schematic diagrams and photograph of the fabricated all-solid-state CuSe NS-SSCs device. (b) CV curves of the device at different scan rates. (c) Galvanostatic CD curves at different current densities. (d) Volume specific capacitances as a function of the current density. (e) Cycle performance of the CuSe NS-SSCs device at a current density of 0.57 mA cm^{-3}. (f) A red LED lamp powered by the tandem of CuSe NS-SSCs devices.

Furthermore, the as-prepared NS-SSCs devices show well flexibility and mechanical stability, and can be bended at different angles (figure S7) without sacrificing the electrochemical performance. **Figure 5** shows the CV curves of CuSe NS-SSCs device bended from 0 degree to 180 degree. The CV curves recorded at different bending angles (90° and 180°) show slight changes compare with the CV curve without bending (0°). The result demonstrates that the CuSe NS films contact well with the Au-coated PET substrate, and the structural integrity of the device is not be destroyed when folded. It should be mentioned that the CV response signal is nearly unchanged even after being folded thousands of times at different bending angles.

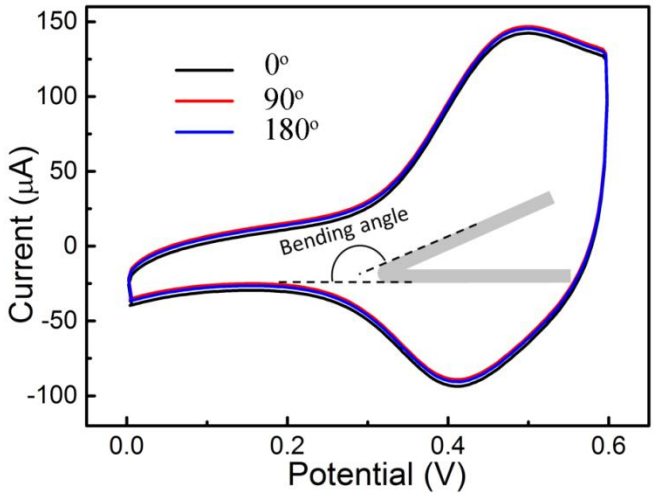

Figure 5. The flexibility and stability of the CuSe NS-SSCs device upon flexing was

evaluated by measuring the CV curves at different bending angles: 0° (black plot), 90° (red plot), and 180° (blue plot).

CONCLUSIONS

In summary, a novel 2D CuSe NS film has been successfully integrated on Au-coated PET substrate for the first time through a facile electrodeposition method after optimizing the deposition parameters. In such NS film, the CuSe NS building blocks are hexagonal klockmannite phase and vertically-oriented on the substrate to form a free-standing film with many macro-pores or open channels. By directly using such CuSe NS film as the electrode, its mass specific capacitance can reach 209 F g^{-1} at a current density of 0.2 A g^{-1}, which is comparable to or higher than those of other reported materials (*e.g.*, G-Mn_3O_4 nanorods, N-doped ultrathin carbon NSs, *etc.*). Such CuSe NS film is further used as electrode to fabricate symmetric, flexible, all-solid-state SCs using PVA-LiCl gel as both the solid electrolyte and the separator. The fabricated solid device exhibits high volumetric specific capacitance (30.17 mF cm^{-3}), good cycling stability, excellent flexibility and desirable mechanical stability. Additionally, as a prototype for practical application, tandem of three such solid devices can light up a red LED for about 3 minutes. This work not only provides an efficient avenue to resolve the spacial orientation problem of CuSe NSs building blocks but also confirms that vertically-oriented and interpenetrating CuSe NS film is an ideal candidate electrode for high-performance, flexible, all-solid-state SCs. Further integrating other electro-active materials (*e.g.* $Ni(OH)_2$, MnO_2, *etc.*) with the CuSe NS films to fabricate advanced hybrid electrode is underway in our lab.

EXPERIMENTAL SECTION

Reagents and materials. The $CuCl_2 \cdot 2H_2O$ (99%), SeO_2 (99%), KCl (99%), LiCl (97%), and HCl (37%) were purchased from Alfa Aesar and directly used without further purification. The polyethylene terephthalate (PET) pieces and polyvinyl alcohol (PVA) were purchased from Zhuhai Kaivo Optoelectronic Technology Co. and Chengdu Kelong Chemical Reagent Co. respectively.

Synthesis of CuSe NS films. CuSe NS films were directly grown on Au-coated PET substrate *via* a facile electrodeposition method. The thickness of the Au film coated on PET pieces is about 80 nm. Before electrodeposition, the electrolyte was prepared by dissolving $CuCl_2 \cdot 2H_2O$ (2 mM), SeO_2 (4.5 mM) and KCl (0.1 M) in 1000 mL distilled water. The pH of the solution was adjusted to 1.5 using 0.2 M HCl solution. The electrodeposition experiments were carried out in a standard three-electrode cell using Au-coated PET piece, Pt sheet and saturated calomel electrode (SCE) as the working electrode, counter electrode, and reference electrode, respectively. The CuSe NS film was prepared under a potentiostatic mode. To obtain high quality NS film, a series of experiments were performed to optimize the deposition parameters. The deposited potentials were varied from -0.02 to -0.20 V (*vs*. SCE), and the deposition temperatures were tuned from 20 to 80 ^{o}C. When the deposition temperature was 60 ^{o}C, a high quality CuSe NS film could be obtained by electrodeposition at -0.15 V (*vs*. SCE) for 30 min.

Materials characterizations. The scanning electron microscope (SEM) images of the CuSe NS films were taken on a scanning electron microscope (FEI quanta 200 and helios 600i),

operating at an accelerating voltage of 20 kV. The transmission electron microscopy (TEM) and high-resolution TEM (HR-TEM) images were performed on FEI, Tecnai F20 transition electron microscopy at an accelerating voltage of 200 kV. The X-ray diffraction (XRD) patterns were recorded on Dandong Comp. TD-3500 diffractometer with Cu Kα radiation (λ = 1.54056 Å). The XPS data were acquired on a scanning X-ray microprobe (PHI 5000 Verasa). Binding energies of Cu 2p and Se 3d were calibrated using $C1_S$ peak (BE = 284.6 eV) as a standard.

Electrochemical tests of CuSe NS films. The electrochemical performance was examined in a three-electrode system and the electrolyte used in the electrochemical measurement was 1 M Na_2SO_4 aqueous solution. The as-prepared CuSe NS film on Au-coated PET substrate, platinum plate, and a saturated calomel electrode (SCE) were used as the working electrode, counter electrode, and reference electrode, respectively. All electrochemical tests were performed on an electrochemical workstation (CHI 660D) at room temperature.

Fabrication and electrochemical tests of flexible all-solid-state SCs. For fabrication of flexible all-solid-state SCs, two pieces of CuSe NS film on Au-coated PET electrodes were immersed in the PVA-LiCl gel solution for 5 min to adsorb a layer of solid electrolyte. After the excess water was vaporized, two pieces of electrodes ated with electrolyte were pressed together and put into a vacuum oven at 50 ^oC for 24 h. Thus, the stacked CuSe NS-SSCs solid devices were fabricated, which were employed to evaluate the supercapacitive performance on an electrochemical workstation (CHI 660D). The PVA-LiCl gel electrolyte was prepared as follows: 6 g of LiCl was added into 60 mL of deionized water, and then 6 g of PVA

powder was added. The whole mixture was heated to 85 ºC under stirring until the solution became clear.

ASSOCIATED CONTENT

Supporting Information Available. This information contains calculation details of the capacitance, SEM images of the samples obtained under other deposition conditions, electrochemical data and structural analysis of CuSe NS film after stability tests, and additional data for flexible all-solid-state devices. This material is available free of charge *via* the Internet at http://pubs.acs.org.

AUTHOR INFORMATION

Corresponding Author

* **Phone/ Fax**: 86-25-85891051

E-mail: jfgong@hhu.edu.cn (Dr. J. F. Gong)

07203@njnu.edu.cn (Prof. Dr. M. Han);

baojianchun@njnu.edu.cn (Prof. Dr. J. C. Bao).

Author Contributions

All authors have given approval to the final version of the manuscript.

Notes

The authors declare no competing financial interest.

Acknowledgements

This work was supported by the National Natural Science Foundation of China for the project (Nos. 21271105, 61176087, 21541007, and 21671106), the Fundamental Research Funds for the Central Universities (Grant Nos. 2015B22313 and 2016B46014), research fund

from the Priority Academic Program Development of Jiangsu Higher Education Institutions, and the opening research foundations of State Key Laboratory of Coordination Chemistry, Nanjing National Laboratory of Solid State Microstructures, Nanjing University.

REFERENCES:

(1) Chmiola, J.; Largeot, C.; Taberna, P. -L.; Simon, P.; Gogotsi, Y. Monolithic Carbide-Derived Carbon Films for Micro-Supercapacitors. *Science* **2010**, *328*, 480-483.

(2) Cao, X.; Yin, Z.; Zhang, H. Three-Dimensional Graphene Materials: Preparation, Structures and Application in Supercapacitors. *Energ. Environ. Sci*. **2014**, *7*, 1850-1865.

(3) Liu, C.; Li, F.; Ma, L. -P.; Cheng, H. -M. Advanced Materials for Energy Storage. *Adv. Mater.* **2010**, *22*, E28.

(4) Jiao, Y.; Liu, Y.; Yin, B.; Zhang, S.; Qu, F.; Wu, X. Hybrid Alpha-Fe_2O_3@NiO Heterostructures for Flexible and High Performance Supercapacitor Electrodes and Visible Light Driven Photocatalysts. *Nano Energy* **2014**, *10*, 90-98.

(5) Yu, D.; Goh, K.; Wang, H.; Wei, L.; Jiang, W.; Zhang, Q.; Dai, L.; Chen, Y. Scalable Synthesis of Hierarchically Structured Carbon Nanotube-Graphene Fibres for Capacitive Energy Storage. *Nat. Nanotech.* **2014**, *9*, 555-562.

(6) Bonaccorso, F.; Colombo, L.; Yu, G.; Stoller, M.; Tozzini, V.; Ferrari, A. C.; Ruoff, R. S.; Pellegrini, V. Graphene, Related Two-Dimensional Crystals, and Hybrid Systems for Energy Conversion and Storage. *Science* **2015**, *347*, 1246501.

(7) Wang, X.; Lu, X.; Liu, B.; Chen, D.; Tong, Y.; Shen, G. Flexible Energy-Storage Devices: Design Consideration and Recent Progress. *Adv. Mater.* **2014**, *26*, 4763-4782.

(8) Lu, X.; Yu, M.; Wang, G.; Tong, Y.; Li, Y. Flexible Solid-State Supercapacitors: Design, Fabrication and Applications. *Energ. Environ. Sci.* **2014**, *7*, 2160-2181.

(9) Kaempgen, M.; Chan, C. K.; Ma, J.; Cui, Y.; Gruner, G. Printable Thin Film Supercapacitors Using Single-Walled Carbon Nanotubes. *Nano Lett.* **2009**, *9*, 1872-1876.

(10) Yu, D.; Dai, L. Self-Assembled Graphene/Carbon Nanotube Hybrid Films for Supercapacitors. *J. Phy. Chem. Lett.* **2010**, *1*, 467-470.

(11) Abioye, A. M.; Ani, F. N. Recent Development in the Production of Activated Carbon Electrodes from Agricultural Waste Biomass for Supercapacitors: A Review. *Renew. Sust. Energ. Rev.* **2015**, *52*, 1282-1293.

(12) Chen, A.; Yu, Y.; Li, Y.; Wang, Y.; Li, Y.; Li, S.; Xia, K. Synthesis of Macro-Mesoporous Carbon Materials and Hollow Core/Mesoporous Shell Carbon Spheres as Supercapacitors. *J. Mater. Sci.* **2016**, *51*, 4601-4608.

(13) Meng, Y.; Zhao, Y.; Hu, C.; Cheng, H.; Hu, Y.; Zhang, Z.; Shi, G.; Qu, L. All-Graphene Core-Sheath Microfibers for All-Solid-State, Stretchable Fibriform Supercapacitors and Wearable Electronic Textiles. *Adv. Mater.* **2013**, *25*, 2326-2331.

(14) Zhu, Y.; Murali, S.; Stoller, M. D.; Ganesh, K. J.; Cai, W.; Ferreira, P. J.; Pirkle, A.; Wallace, R. M.; Cychosz, K. A.; Thommes, M.; Su, D.; Stach, E. A.; Ruoff, R. S. Carbon-Based Supercapacitors Produced by Activation of Graphene. *Science* **2011**, *332*, 1537-1541.

(15) Fan, Z.; Yan, J.; Zhi, L.; Zhang, Q.; Wei, T.; Feng, J.; Zhang, M.; Qian, W.; Wei, F. A Three-Dimensional Carbon Nanotube/Graphene Sandwich and Its Application as Electrode in Supercapacitors. *Adv. Mater.* **2010**, *22*, 3723.

(16) Chen, P.; Chen, H.; Qiu, J.; Zhou, C. Inkjet Printing of Single-Walled Carbon Nanotube /RuO_2 Nanowire Supercapacitors on Cloth Fabrics and Flexible Substrates. *Nano Res.* **2010**, *3*, 594-603.

(17) Wang, P.; Xu, Y.; Liu, H.; Chen, Y.; Yang, J.; Tan, Q. Carbon/Carbon Nanotube-Supported RuO_2 Nanoparticles with a Hollow Interior as Excellent Electrode Materials for Supercapacitors. *Nano Energy* **2015**, *15*, 116-124.

(18) Gao, Z. -D.; Zhu, X.; Li, Y. -H.; Zhou, X.; Song, Y. -Y.; Schmuki, P. Carbon Cladded TiO_2 Nanotubes: Fabrication and Use in 3D-RuO_2 based Supercapacitors. *Chem. Commun.* **2015**, *51*, 7614-7617.

(19) Bao, J.; Zhang, X.; Bai, L.; Bai, W.; Zhou, M.; Xie, J.; Guan, M.; Zhou, J.; Xie, Y. All-Solid-State Flexible Thin-Film Supercapacitors with High Electrochemical Performance Based on a Two-Dimensional V_2O_5/Graphene Composite. *J. Mater. Chem. A.* **2014**, *2*, 10876-10881.

(20) Wang, J. -G.; Kang, F.; Wei, B. Engineering of MnO_2-Based Nanocomposites for High-Performance Supercapacitors. *Prog. Mater. Sci.* **2015**, *74*, 51-124.

(21) Cao, J.; Li, X.; Wang, Y.; Walsh, F. C.; Ouyang, J. -H.; Jia, D.; Zhou, Y. Materials and Fabrication of Electrode Scaffolds for Deposition of MnO_2 and Their True Performance in Supercapacitors. *J. Power Sources* **2015**, *293*, 657-674.

(22) Wang, L.; Deng, D.; Salley, S. O.; Ng, K. Y. S. Facile Synthesis of 3D Composites of MnO_2 Nanorods and Holey Graphene Oxide for Supercapacitors. *J. Mater. Sci.* **2015**, *50*, 6313-6320.

(23) Yan, J.; Fan, Z.; Sun, W.; Ning, G.; Wei, T.; Zhang, Q.; Zhang, R.; Zhi, L.; Wei, F. Advanced Asymmetric Supercapacitors Based on $Ni(OH)_2$/Graphene and Porous Graphene Electrodes with High Energy Density. *Adv. Funct. MateR.* **2012**, *22*, 2632-2641.

(24) Xiong, X.; Ding, D.; Chen, D.; Waller, G.; Bu, Y.; Wang, Z.; Liu, M. Three-Dimensional Ultrathin $Ni(OH)_2$ Nanosheets Grown on Nickel Foam for High-Performance Supercapacitors. *Nano Energy* **2015**, *11*, 154-161.

(25) Hu, C. -C.; Chen, J. -C.; Chang, K. -H. Cathodic Deposition of $Ni(OH)_2$ and $Co(OH)_2$ for Asymmetric Supercapacitors: Importance of the Electrochemical Reversibility of Redox Couples. *J. Power Sources* **2013**, *221*, 128-133.

(26) Feng, J. X.; Ding, L. X.; Ye, S. H.; He, X. J.; Xu, H.; Tong, Y. X.; Li, G. R. $Co(OH)_2$@ PANI Hybrid Nanosheets with 3D Networks as High-Performance Electrocatalysts for Hydrogen Evolution Reaction. *Adv. Mater.* **2015**, *27*, 7051.

(27) Feng, J.; Sun, X.; Wu, C.; Peng, L.; Lin, C.; Hu, S.; Yang, J.; Xie, Y. Metallic Few-Layered VS_2 Ultrathin Nanosheets: High Two-Dimensional Conductivity for In-Plane Supercapacitors. *J. Am. Chem. Soc.* **2011**, *133*, 17832-17838.

(28) Cao, L.; Yang, S.; Gao, W.; Liu, Z.; Gong, Y.; Ma, L.; Shi, G.; Lei, S.; Zhang, Y.; Zhang, S.; Vajtai, R.; Ajayan, P. M. Direct Laser-Patterned Micro-Supercapacitors from Paintable MoS_2 Films. *Small* **2013**, *9*, 2905-2910.

(29) Choudhary, N.; Patel, M.; Ho, Y. -H.; Dahotre, N. B.; Lee, W.; Hwang, J. Y.; Choi, W. Directly Deposited MoS_2 Thin Film Electrodes for High Performance Supercapacitors. *J. Mater. Chem. A* **2015**, *3*, 24049-24054.

(30) Krishnamoorthy, K.; Veerasubramani, G. K.; Pazhamalai, P.; Kim, S. J. Designing Two Dimensional Nanoarchitectured MoS_2 Sheets Grown on Mo Foil as a Binder Free Electrode for Supercapacitors. *Electrochim. Acta* **2016**, *190*, 305-312.

(31) Liu, Y.; Wang, W.; Huang, H.; Gu, L.; Wang, Y.; Peng, X. The Highly Enhanced Performance of Lamellar WS_2 Nanosheet Electrodes upon Intercalation of Single-Walled Carbon Nanotubes for Supercapacitors and Lithium Ions Batteries. *Chem. Comm.* **2014**, *50*, 4485-4488.

(32) Hu X., Shao W., Hang X. D., Zhang X. D., Zhu W. G., Xie Y. Superior Electrical Conductivity in Hydrogenated Layered Ternary Chalcogenide Nanosheets for Flexible All-Solid-State Supercapacitors. *Angew. Chem. Inter. Ed.* **2016**, *128*, 5827-5832.

(33) Zhang, C. L.; Yin, H. H.; Han, M.; Dai, Z. H.; Pang, H.; Zheng, Y. L.; Lan, Y. -Q.; Bao, J. C.; Zhu, J. M. Two-Dimensional Tin Selenide Nanostructures for Flexible All-Solid-State Supercapacitors. *ACS Nano* **2014**, *8*, 3761-3770.

(34) Hamilton, C. E.; Flood, D. J.; Barron, A. R. Thin Film CdSe/CuSe Photovoltaic on a Flexible Single Walled Carbon Nanotube Substrate. *Phys. Chem. Chem. Phys.* **2013**, *15*, 3930 -3938.

(35) Seo, Y. -H.; Lee, B. -S.; Jo, Y.; Kim, H. -G.; Choi, Y.; Ahn, S.; Yoon, K.; Woo, K.; Moon, J.; Ryu, B. -H.; Jeong, S. Facile Microwave-Assisted Synthesis of Multiphase $CuInSe_2$ Nanoparticles and Role of Secondary CuSe Phase on Photovoltaic Device Performance. *J. Phys. Chem. C* **2013**, *117*, 9529-9536.

(36) Xu, J.; Zhang, W.; Yang, Z.; Ding, S.; Zeng, C.; Chen, L.; Wang, Q.; Yang, S.

Large-Scale Synthesis of Long Crystalline $Cu_{2-x}Se$ Nanowire Bundles by Water-Evaporation -Induced Self Assembly and Their Application in Gas Sensing. *Adv. Funct. Mater.* **2009**, *19*, 1759-1766.

(37) Seo, Y. -H.; Lee, B. -S.; Jo, Y.; Kim, H. -G.; Woo, K.; Moon, J.; Choi, Y.; Ryu, B. -H.; Jeong, S. Study on Thermal Evolution of the CuSe Phase in Nanoparticle-Based Absorber Layers for Solution-Processed Chalcopyrite Photovoltaic Devices. *ACS Appl. Mater. Interfaces* **2013**, *5*, 6930-6936.

(38) Gu, Y. J.; Su, Y. J.; Chen, D.; Geng, H. J.; Li, Z. L.; Zhang, L. Y.; Zhang, Y. F. Hydrothermal Synthesis of Hexagonal CuSe Nanoflakes with Excellent Sunlight-Driven Photocatalytic Activity. *CrystEngCommun.* **2014**, *16*, 9185-9190.

(39) Wu, X. J.; Huang, X.; Liu, J. Q.; Li, H.; Yang, J.; Li, B.; Huang, W.; Zhang, H. Two-Dimensional CuSe Nanosheets with Microscale Lateral Size: Synthesis and Template-Assisted Phase Transformation. *Angew. Chem. Inter. Ed.* **2014**, *53*, 5083-5087.

(40) Vikulov, S.; Di Stasio, F.; Ceseracciu, L.; Saldanha, P. L.; Scarpellini, A.; Dang, Z. Y.; Krahne, R.; Manna, L.; Lesnyak, V. Fully Solution-Processed Conductive Films Based on Colloidal Copper Selenide Nanosheets for Flexible Electronics. *Adv. Funct. Mater.* **2016**, *26*, 3670-3677.

(41) Liu, Y. Q.; Wang, F. X.; Xiao, Y.; Peng, H. D.; Zhong, H. J.; Liu, Z. H.; Pan, G. B. Facile Microwave-Assisted Synthesis of Klockmannite CuSe Nanosheets and Their Exceptional Electrical Properties. *Sci. Rep.* **2014**, *4*, 5998.

(42) Liu, Y. Q.; Wu, H. D.; Zhao, Y.; Pan, G. B. Metal Ions Mediated Morphology and Phase

Transformation of Chalcogenide Semiconductor: From $CuClSe_2$ Microribbon to CuSe Nanosheet. *Langmuir* **2015**, *31*, 4958-4963.

(43) Lee, J. W.; Hall, A. S.; Kim, J. D.; Mallouk, T. E. A Facile and Template-Free Hydrothermal Synthesis of Mn_3O_4 Nanorods on Graphene Sheets for Supercapacitor Electrodes with Long Cycle Stability. *Chem. Mater.* **2012**, *24*, 1158-1164.

(44) Zhu, S.; Li, J.; Ma, L.; Guo, L.; Li, Q.; He, C.; Liu, E.; He, F.; She, C.; Zhao, N. Three-Dimensional Network of N-Doped Carbon Ultrathin Nanosheets with Closely Packed Mesopores: Controllable Synthesis and Application in Electrochemical Energy Storage. *ACS Appl. Mater. Interfaces* **2016**, *8*, 11720-11728.

(45) Sakr, G. B.; Yahia, I. S.; Fadel, M.; Fouad, S. S.; Romcevic, N. Optical Spectroscopy, Optical Conductivity, Dielectric Properties and New Methods for Determining the Gap States of CuSe Thin Films. *J. Alloy. Compd.* **2010**, *507*, 557-562.

(46) Zhang, S. -Y.; Fang, C. -X.; Tian, Y. -P.; Zhu, K. -R.; Jin, B. -K.; Shen, Y. -H.; Yang, J. -X. Synthesis and Characterization of Hexagonal CuSe Nanotubes by Templating against Trigonal Se Nanotubes. *Cryst. Growth. Des.* **2006**, *6*, 2809-2813.

(47) Zhang, Y.; Qiao, Z. P.; Chen, X. M. Microwave-Assisted elemental direct reaction route to nanocrystalline copper chalcogenides CuSe and Cu_2Te. *J. Mater. Chem.* **2002**, *12*, 2747-2748.

(48) Wang, B.; Park, J.; Su, D. W.; Wang, C. Y.; Ahn, H.; Wang, G. X. Solvothermal Synthesis of CoS_2-Graphene Nanocomposite Material for High-Performance Supercapacitors. *J. Mater. Chem.* **2012**, *22*, 15750-15756.

(49) Mai, L. Q.; Yang, F.; Zhao, Y. L.; Xu, X.; Xu, L.; Luo, Y. Z. Hierarchical $MnMoO_4$/ $CoMoO_4$ Heterostructured Nanowires with Enhanced Supercapacitor Performance. *Nat. Commun.* **2011**, *2*, 381.

(50) Pang, H.; Liu, Y. Y.; Li, J.; Ma, Y. H.; Li, G. C.; Ai, Y. N.; Chen, J.; Zhang, J. S.; Zheng, H. H. Cobalt Phosphite Microarchitectures Assembled by Ultralong Nanoribbons and Their Application as Effective Electrochemical Capacitor Electrode Materials. *Nanoscale* **2013**, *5*, 503-507.

TOC GTAPHICS